AJRCMB Articles in Press. Published on 05-January-2016 as 10.1165/rcmb.2015-0014OC

Hydrogen sulfide prevents and partially reverses ozone-induced feature of lung inflammation and emphysema in mice

Feng Li[1*], Pengyu Zhang[1*], Min Zhang[1*], Li Liang[3], Xiaoyuan Sun[1], Min Li[2],Yueqin Tang[2], Aihua Bao[1], Jicheng Gong[4], Junfeng (Jim) Zhang[4], Ian Adcock[5], Kian Fan Chung[5], Xin Zhou[1#]

1. Dept of Respiratory Medicine, Shanghai First People's Hospital, Shanghai Jiaotong University, Shanghai, 200080, P.R. China
2. Experimental Research Center, Shanghai First People's Hospital, Shanghai Jiaotong University, Shanghai, 200080, P.R. China
3. Dept of Respiratory Medicine, Shanghai Third People's Hospital, Shanghai Jiaotong University School of Medicine, Shanghai, 201999, P.R. China
4. Division of Environmental Sciences & Policy, Nicholas School of the Environment & Duke Global Health Institute, Duke University, Durham, NC 27708, USA
5. Airway Diseases Section, National Heart and Lung Institute, Imperial College London, London, SW3 6LY, UK

Author Contributions:

FL,IA,KFC,XZ conceived and designed the study. FL,PZ,YT carried out the animal exposure studies. FL,PZ,MZ did Mciro-CT scanning and measured lung function. LL, XS, ML, AB performed molecular biological experiments. JG,JZ performed HPLC analysis. FL,PZ prepared the manuscript. XZ, JZ, KFC analyzed data and contributed to manuscript revision.

Runing title: Effects of hydrogen sulfide on ozone-induced COPD

*These authors contributed equally to this work.

[#]Corresponding author:

Professor Xin Zhou

Dept of Respiratory Medicine,

Shanghai First People's Hospital, Shanghai Jiao Tong University.

No.100, Haining Road, Shanghai, 200080, China.

E-mail: xzhou53@163.com

Telephone number: 0086 21 63071428

Fax number: 0086 21 63071428

AJRCMB Articles in Press. Published on 05-January-2016 as 10.1165/rcmb.2015-0014OC

Abstract

Hydrogen sulfide (H_2S), a novel signaling gasotransmitter in the respiratory system, may have anti-inflammatory properties in the lung. We examined the preventive and therapeutic effects of H_2S on ozone-induced feature of lung inflammation and emphysema. C57/BL6 mice were exposed to ozone or filtered air over 6 weeks. Sodium hydrogen sulfide (NaHS), a H_2S donor, was administered to the mice either before ozone exposure (preventive effect) or after completion of ozone exposure for 6 weeks (therapeutic effect). The ozone-exposed mice developed emphysema measured by micro-computed tomography and histology, airflow limitation measured by the forced maneuver system, and increased lung inflammation with augmented IL-1β, IL-18 and MMP-9 gene expression. Ozone-induced changes were associated with increased NLRP3-caspase-1 activation and p38 MAPK phosphorylation and decreased Akt phosphorylation. NaHS both prevented and reversed lung inflammation and emphysematous changes in alveolar space. In contrast, NaHS prevented but did not reverse ozone-induced airflow limitation and bronchial structural remodeling. In conclusion, NaHS administration prevented and partially reversed ozone-induced feature of lung inflammation and emphysema via regulation of the NLRP3-caspase-1, p38 MAPK and Akt pathways.

Key words:

hydrogen sulfide, ozone exposure, lung inflammation and emphysema

Introduction

Chronic obstructive pulmonary disease (COPD) is an increasing cause of morbidity and mortality worldwide and is characterized by chronic inflammation and alveolar destruction (emphysema), which ultimately contributes to irreversible airflow obstruction (1). Besides cigarette smoke, other risk factors including indoor/outdoor air pollution and occupational exposure are also associated with the development of COPD. Oxidative stress, due to the overproduction of exogenous or endogenous oxidants and/or impairment in antioxidant defenses, is a major predisposing factor in the pathogenesis of COPD (2).

As a main environmental pollutant, ozone can directly react with respiratory tract lining fluid contents to produce the secondary reactive oxygen species (ROS) and subsequently activate the signaling pathways or transcription factors to initiate oxidative damage to the lung tissue (3) . Exposure to levels of ozone as encountered on days of high urban pollution has been linked to worsening symptoms and increased hospitalizations in patients with COPD (4-6) . Repeated exposure to high concentrations of ozone in mice has been shown to cause chronic lung inflammation, emphysema and airflow limitation, mimicking features of COPD.These features were neither prevented nor reversed by treatment with N-acetylcysteine, a commonly used antioxidant in the clinic (7).

Hydrogen sulfide (H_2S), a gas with the odor of rotten eggs, is catalyzed in

AJRCMB Articles in Press. Published on 05-January-2016 as 10.1165/rcmb.2015-0014OC

the body from cysteine mainly by cystathionine-γ-lyase (CSE) and cystathionine-β-synthetase (CBS), and also by 3-mercaptopyruvate sulfur transferase (MST) (8). H_2S is recognized as the third signaling gasotransmitter after carbon monoxide (CO) and nitric oxide (NO). H_2S may regulate physiological functions such as airway constriction, cell proliferation and apoptosis in the lungs, and may also be involved in pathophysiological mechanisms underlying many respiratory diseases (8). In COPD, serum H_2S levels were higher in patients with stable COPD (S-COPD) than those in patients with acute exacerbation of COPD (AECOPD) (9). However, sputum H_2S levels were higher in AECOPD patients than those in S-COPD patients, such that a high sputum-to-serum ratio of H_2S has been related to ongoing neutrophilic inflammation (10). H_2S may possess anti-inflammatory and anti-remodeling roles in COPD. Experimentally, sodium hydrogen sulfide (NaHS), a donor of H_2S, has been shown to inhibit airway hyperresponsiveness (11), reduce airway inflammation and prevent emphysema in a cigarette smoke-induced COPD model (12).

We hypothesized that exogenous NaHS prevents and reverses ozone-induced features of COPD, namely lung inflammation and emphysema. Hence, in the present study, we evaluated both the preventive and therapeutic effects of H_2S delivered as NaHS on inflammation, emphysema, pulmonary function, and inflammatory gene expression in an ozone-induced murine model of lung inflammation and emphysema. We also determined the

underlying intracellular signaling pathways that may be affected by H_2S.

Material and methods

A detailed description is available in the online supplement.

Ozone exposure

C57/BL6 mice were exposed to ozone (2.5 parts per million) or filtered air for 3 hours, twice a week, over 6 weeks. NaHS (2mg/kg) or PBS was administered intraperitoneally to mice either before each exposure or after cessation of exposure twice a week for 6 weeks (Supplemental Figure S1).

Micro-computed tomography (micro-CT)

Mice were anesthetised and placed in the chamber of the Micro-CT eXplore Locus (GE healthcare, London, Ontario, Canada). Images were acquired, reconstructed and analyzed using Microview 2.0 +ABA software. The low attenuation area (LAA) was set in the range of -750 to -550 Hounsfield Units (HU). The percentage of LAA (LAA%) was calculated using the ratio of LAA volume to total lung volume.

Lung function

Mice were placed in a whole-body plethysmograph (Buxco,Wilmington, NC,USA) to measure inspiratory capacity (IC), functional residual capacity (FRC), total lung capacity (TLC),forced vital capacity (FVC) , forced expiratory volume in first 25 and 50 milliseconds of exhalation (FEV_{25}, FEV_{50}) and chord compliance (Cchord).

Bronchoalveolar lavage fluid and blood collection

AJRCMB Articles in Press. Published on 05-January-2016 as 10.1165/rcmb.2015-0014OC

Following terminal anaesthesia, bronchoalveolar lavage (BAL) fluid and blood were collected. Total cell counts and differential cell counts were determined. BAL malondialdehyde (MDA) was measured using a HPLC system and serum 8-hydroxy-2'-deoxyguanosine (8-OHdG) was analyzed using a HPLC-MS-MS technique.

Histology

Lung sections were stained with haematoxylin and eosin (H&E). The mean linear intercept (Lm) was determined by dividing the length of the line in a reticule by the number of alveolar wall and grid line interception. Lung inflammatory response was scored on a 0–3 scale. The components of airway structure were calculated through dividing the length of the perimeter of basement membrane (Pbm) by the area of airway epithelium (Wae), airway smooth muscle (Wam) and total airway wall (Wat).

Lung sections were blocked and then incubated with polyclonal rabbit anti-active caspase-3 (Cell Signaling Technology, Beverly, CA, USA) for immunostaining. The active caspase-3-positive stained cells per field were counted under the microscope.

Polymerase chain reaction (PCR)

Total RNA was extracted from frozen lung tissue using Trizol and then reverse-transcripted to cDNA. The real-time PCR analyses were conducted using SYBR Green PCR supermix reagent and Step one plus system(Life Technologies, South San Francisco, CA,USA). The relative abundance of gene

expression of IL-1β, IL-18, MMP-9, SOD2 and HO-1 was normalized to beta-actin expression.

Western blot

Frozen lung tissues were homogenized in RIPA buffer and total protein concentrations were quantified by BCA analysis. Equal amounts of protein were separated by SDS-PAGE and electrophoretically transferred to nitrocellulose membranes. The membranes were blocked, then incubated with primary antibodies against NLRP3, caspase-1 (Adipogen, San Diego,CA,USA), phospho-Akt, total Akt, phospho-p38 MAPK, total p38 MAPK and GAPDH (Cell Signaling Technology, Beverly, CA, USA), for blot detection.

Statistical analysis

All results were expressed as mean ± S.E.M. One-way analysis of variance (ANOVA) with Bonferroni post test or Dunnett T3 post test was performed for comparisons between multiple groups using SPSS 20.0 software. $P<0.05$ was considered significant.

Results:

1.Micro-CT analysis and Lm

Examples of micro-CT pictures are shown in Figures 1A-1H. There were significant increases in CT-derived total lung volume and LAA% in ozone-exposed mice and remained increased after 6 weeks of ozone cessation. (Figures 1I-1J). Both preventive NaHS treatment and therapeutic NaHS treatment in ozone-exposed mice led to a reduction in total lung volume

AJRCMB Articles in Press. Published on 05-January-2016 as 10.1165/rcmb.2015-0014OC

and LAA%.

Examples of lung alveolar enlargement after ozone exposure are shown in Figures 2A-2H. An increase in Lm was observed in ozone-exposed mice and persisted after 6 weeks of ozone exposure cessation (Figure 2I and 2J). Both preventive and therapeutic NaHS intervention inhibited Lm. There was a positive correlation between CT-derived whole lung volume and Lm ($r=0.5428$; $p<0.001$).

2. Lung function

Lung volume parameters (IC, FRC and TLC) and compliance (Cchord) were increased and airflow rate during expiration (FEV_{25}/FVC, FEV_{50}/FVC) were decreased in ozone-exposed mice (Figures 3A-3F).These values remained unchanged up to 6-week after cessation of ozone exposure. Preventive NaHS treatment inhibited the increases in FRC and TLC, and prevented the decreases in FEV_{25}/FVC and FEV_{50}/FVC, while therapeutic NaHS treatment only reduced FRC and TLC (Figures 3A-3F).

3. BAL cells and lung inflammation scores

The BAL total cell counts, including macrophages, lymphocytes, neutrophils and eosinophils, were increased in ozone-exposed mice (Figures 3A-3E). Preventive treatment with NaHS decreased lymphocyte, neutrophil and eosinophil numbers, and therapeutic treatment with NaHS did not affect total or differential cell counts (Figures 4A-4E).

Increased lung inflammation scores with peribronchial and perivascular

inflammatory cell infiltrates in lung sections were observed in ozone-exposed mice(Figure 4F). This inflammatory response persisted up to 6 weeks after cessation of ozone exposure. Both preventive and therapeutic treatment with NaHS reduced lung inflammation scores (Figure 4F).

Total cell counts were positively correlated with TLC ($r=0.4164, P<0.001$) and Cchord ($r=0.278, P<0.05$), and negatively correlated with FEV_{25}/FVC ($r=0.2654, P<0.05$). The numbers of macrophages and lymphocytes were positively correlated with TLC ($r=0.4001, P<0.01$; $r=0.3567, P<0.01$). The numbers of neutrophils were positively correlated with Cchord ($r=0.2639, P<0.05$).

Inflammation scores were positively correlated with TLC ($r=0.4903, P<0.001$), FRC ($r=0.3169, P<0.05$),and Cchord ($r=0.4988, P<0.001$), and negatively correlated with FEV_{25}/FVC ($r=0.4454, P<0.001$) and FEV_{50}/FVC ($r=0.253, P<0.05$). Inflammation scores were also positively correlated to LAA% ($r=0.4511, P<0.001$).

4. Oxidant markers

There was no increase in BAL MDA in ozone-exposed mice compared to control mice. Preventive and therapeutic NaHS treatment did not affect MDA concentrations (Figure 4G). Ozone exposure increased the levels of serum 8-OHdG compared to control mice. Preventive but not therapeutic intervention with NaHS reduced serum 8-OHdG levels (Figure 4H).

Both contents of BAL MDA and serum 8-OHdG were positively correlated

AJRCMB Articles in Press. Published on 05-January-2016 as 10.1165/rcmb.2015-0014OC

with Cchord (r=0.2591,P<0.05; r=0.2632,P<0.05), inflammation scores (r=0.3223,P<0.01; r=0.2869,P<0.05) and caspase-3 positive cells (r=0.2475,P<0.05; r=0.2947,P<0.05). Serum 8-OHdG were positively correlated with the numbers of neutrophils (r=0.2607,P<0.05), lymphocytes (r=0.2840,P<0.05) and eosinophils (r=0.3188,P<0.05).

5.Bronchial wall remodeling

Ozone exposure led to increases in airway epithelial layer, airway smooth muscle (ASM) and total airway wall compared to control mice (Figures 5A-5C). The thickness of ASM remained increased, while the thickness in airway epithelial layer and total airway wall recovered to normal after 6-week of ozone cessation. Preventive NaHS treatment decreased the thickness of airway epithelial layer, ASM and total airway wall, while the therapeutic NaHS treatment showed no effect(Figures 5A-5C).

6.Active caspase-3 cells

Increased active caspase-3-positive cells were observed in airway epithelial cells, alveolar type II epithelial cells and monocytes /macrophages of the lung parenchyma in ozone-exposed mice compared to control mice, and remained increased after 6 weeks of ozone cessation. Both preventive and therapeutic treatment with NaHS reduced the number of caspase-3-postive cells in the lung parenchyma (Figure 5D). Examples of caspase-3-postive cells in the lung are shown in Supplemental Figure S2.

7.mRNA expression in lungs

Ozone exposure induced the mRNA expression of IL-1β, IL-18 and MMP-9 in the lung tissue (Figures 6A-6E). Preventive NaHS intervention decreased the mRNA levels of IL-1β, IL-18, MMP-9, and enhanced SOD2 and HO-1 mRNA expression, while therapeutic NaHS intervention decreased mRNA levels of IL-1β and IL-18 (Figures 6A-6E).

8.NLRP3 expression, caspase-1 activation, p38 MAPK and Akt phosphorylation

Ozone exposure increased NLRP3 protein expression and the ratio of cleaved caspase-1 to pro-caspase-1, which remained increased after 6 weeks of ozone cessation. Preventive and therapeutic treatment with NaHS decreased NLRP3 protein level and the ratio of cleaved caspase-1 to pro-caspase-1 in ozone-exposed mice (Figures 7A and 7B).

Ozone exposure caused an induction of p38 MAPK phosphorylation and a reduction of Akt phosphorylation, both of which remained unchanged after 6-week of ozone cessation. Both preventive and therapeutic treatment with NaHS reduced the phosphorylation of p38 MAPK and stimulated the phosphorylation of Akt in ozone-exposed mice (Figures 7C and 7D).

Both NLRP3 expression and the ratios of phospho-p38 MAPK/p38 MAPK were positively correlated with total cells ($r=0.3929, P<0.01$; $r=0.3507, P<0.01$), the numbers of macrophages ($r=0.3080, P<0.05$; $r=0.2678, P<0.05$), neutrophils ($r=0.4624, P<0.001$; $r=0.4559, P<0.001$) and eosinophils ($r=0.4531, P<0.001$; $r=0.3696, P<0.01$), and inflammation scores ($r=0.7363, P<0.001$;

AJRCMB Articles in Press. Published on 05-January-2016 as 10.1165/rcmb.2015-0014OC

r=0.4012,P<0.01). The ratios of cleaved-caspase-1/pro-caspase-1 were positively correlated with inflammation scores (r=0.5314,P<0.001). The ratios of phospho-Akt/Akt were negatively correlated with the numbers of neutrophils (r=-0.2530,P<0.05) and eosinophils (r=-0.2815,P<0.05), and inflammation scores (r=-0.3636,P<0.01).

NLRP3 expression was positively correlated with LAA% (r=0.4064,P<0.001), the numbers of caspase-3 positive cells (r=0.6459,P<0.001), Wam/Pbm (r=0.4122,P<0.001), and Wat/Pbm (r=0.3132,P<0.05). The ratios of cleaved-caspase-1/pro-caspase-1 were positively correlated with LAA% (r=0.6127,P<0.001), Lm (r=0.4153,P<0.001), the numbers of caspase-3 positive cells (r=0.4804,P<0.001) and Wam/Pbm (r=0.3634,P<0.01). The ratios of phospho-P38 MAPK/P38 MAPK were positively correlated with the numbers of caspase-3 positive cells (r=0.4004,P<0.001), Wam/Pbm (r=0.3143,P<0.05). The ratios of phospho-Akt/Akt were negatively correlated with LAA% (r=0.4506,P<0.001), Lm (r=0.2533,P<0.05), the numbers of caspase-3 positive cells (r=0.4434,P<0.001), Wae/Pbm (r=0.4127,P<0.001), Wam/Pbm (r=0.3496,P<0.01), and Wat/Pbm (r=0.39,P<0.01).

Discussion

In the present study, preventive treatment with NaHS inhibited multiple ozone-induced lung inflammation, airway remodeling, emphysema, airflow

limitation and oxidative stress, while therapeutic treatment with NaHS reversed emphysema but not airflow obstruction. Furthermore, both the preventive and therapeutic NaHS treatments inhibited NLRP3 expression and caspase-1 activation, inhibited p38 MAPK phosphorylation and increased Akt phosphorylation. Thus, we conclude that H_2S protects and partially reverses multiple ozone exposure induced lung inflammation and emphysema via its regulation of the NLRP3-caspase-1, p38 MAPK and Akt pathways.

Mutiple ozone exposure caused lung inflammation as indicated by increased macrophages, lymphocytes, neutrophils and eosinophils in the BAL fluid, and inflammatory scores in the lung sections. H_2S has been shown to be pro-inflammatory in various models such as acute pancreatitis associated lung injury (13), burn injury (14), and endotoxic shock (15). On the other hand, H_2S has anti-inflammatory effects on models of acute lung injury (16), asthma (17-19) and COPD (12). Our recent study in an acute ozone exposure model showed that NaHS inhibited airway inflammation by reducing BAL inflammatory cells and lung pro-inflammatory cytokines (20). We now demonstrate that NaHS decreased BAL inflammatory cells, lung inflammation scores and mRNA levels of IL-1β, IL-18 and MMP-9 in the lung, indicating an anti-inflammatory effect of H_2S in the multiple ozone exposure model.

The induction of emphysema by multiple ozone exposure was confirmed by the micro-CT and Lm measurements that provide a measure of air-space enlargement. As a non-invasive measurement, micro-CT is ideal for

AJRCMB Articles in Press. Published on 05-January-2016 as 10.1165/rcmb.2015-0014OC

quantification of emphysema because of the inherent contrast between tissue and air that exists in the lung (21). Increased lung volume (i.e, hyper-inflated lung) was observed in multiple ozone-exposed mice, measured both by micro-CT scan and by body plethysmography. Lm has been used as a measure of alveolar size. However, Lm is an *ex vivo* measurement made on the lung slices and could be affected by many factors (22). The advantages of micro-CT include its ability to assess the lung in its entirety, even in three-dimensional model and can be repeated over time. Our study showed that micro-CT derived total lung volume was moderately correlated with Lm. Using the definition of LAA(23, 24), we compared LAA% in the different groups. Enhanced LAA% in the lung of multiple ozone exposed mice indicates an emphysematous change. Apoptosis is an important factor in the pathogenesis of COPD and contributes to emphysematous lung destruction. An increased number of active caspase-3 positive cells, a sign of apoptosis, was found in the lung alveolar septal space of multiple ozone-exposed mice. Thus, the development of ozone-induced emphysema is likely to be secondary to the activation of apoptotic mechanisms in respiratory alveolar cells. NaHS both prevented and reversed the development of emphysema with preservation of lung volume and a decrease in the number of active caspase-3 positive cells, indicating another potential mechanism of H_2S.

It has been demonstrated that chronic exposure to ozone could cause airway functional impairment in both children and young adults (25,26). We

noted lung hyperinflation as denoted by the increased IC, FRC and TLC, an effect likely to be associated with loss of lung elastic recoil as measured by the increased Cchord, and airflow obstruction indicated by the decreases in FEV_{25}/FVC and FEV_{50}/FVC in multiple ozone exposed mice. These functional changes were similar to those reported in the elastase-induced emphysema mouse model (27).The airflow obstruction in multiple ozone exposed mice could be related to emphysema, small airway remodelling and airway/lung inflammation. Both preventive and therapeutic NaHS treatment prevented the lung hyperinflation in terms of changes in FRC and TLC. However, only preventive treatment, but not therapeutic treatment with NaHS improved the airflow indices, i.e. FEV_{25}/FVC and FEV_{50}/FVC. This may be due to the fact that therapeutic NaHS showed less effect in reversing small airway remodeling (especially the increased mass of airway smooth muscle)

Other studies of chronic ozone exposure have reported different effects on lung function. Increased chest wall compliance and IC were observed in the macaque monkey seasonally exposed to ozone (0.25ppm) for 18 months (28). A reduction in residual volume (RV) was found in the F344/N rat that were exposed to 0.5ppm of ozone for 20 months (29). In the Hartley guinea pig, one week of ozone exposure (ranging from 0.2 to 0.8ppm) resulted in decreases in TLC, vital capacity(VC) and lung compliance, while ozone exposure also led to increases in FEV rates, RV and end-expiratory volume(EEV), which may be suggestive of pulmonary gas-trapping (30). In these studies, lower

AJRCMB Articles in Press. Published on 05-January-2016 as 10.1165/rcmb.2015-0014OC

concentrations of ozone of similar levels found in polluted urban areas were used and did not cause emphysema but induced bronchiolitis and fibrosis of the airways. That explained the reduction in lung compliance and increases in lung volume reported. In our model, we specifically used higher levels of ozone exposure to induce emphysema and lung inflammation, which may explain the differences observed in our study compared to the other studies.

Oxidative stress, characterized by an altered redox regulation with increased ROS, is a major mechanism underlying ozone-induced lung injury. ROS reacts with cell lipid membranes to form stable products including MDA, and with DNA to form products including 8-OHdG. Previously, we showed that acute ozone exposure increased both BAL total MDA and serum 8-OHdG (20). In the present study, however, multiple ozone exposure induced an increase in serum 8-OHdG, but not in BAL MDA. This suggests that multiple ozone exposure induces a systemic oxidative stress, as we observed the increased oxidative stress levels in the serum but not in the BAL fluid. The contents of both BAL MDA and serum 8-OHdG were positively correlated with inflammation scores and the numbers of caspase-3 positive cells, and serum 8-OHdG concentrations were positively correlated with BAL neutrophils, lymphocytes and eosinophils, which suggests that oxidative stress is an important mechanism for multiple ozone induced lung inflammation and emphysema. On the other hand, multiple ozone exposure can activate antioxidant defenses, which may act to curtail the oxidant effects of ozone. We

now show that treatment with NaHS prior to ozone exposure prevented the increase in serum 8-OHdG, indicative of a ROS scavenging effect by H_2S, which is consistent with the finding of a previous study (31). H_2S has also been shown to increase the expression and activity of antioxidant enzymes, such as superoxide dismutase and glutathione peroxidase (19). Our study showed that the preventive NaHS treatment increased mRNA expression of superoxide dismutase 2 (SOD2) and heme oxygenase-1 (HO-1), which could underlie the anti-oxidant mechanism of H_2S in our model.

NLRP3 inflammasome is an intracellular danger-sensing protein complex, which includes the NLRP3 and inactive pro-caspase-1. After activation by signals such as intracellular ROS, NLRP3 could induce caspase-1 auto-cleavage, leading to the secretion of IL-1β and IL-18. NLRP3 may play a key role in the pathogenesis of COPD (32, 33). Previous studies have reported that IL-1β and IL-18 were increased in the lung tissue of COPD patients (34, 35). Eltom etal found that increased caspase-1 activity was present in lungs of smokers and patients with emphysema (36). We now demonstrate that multiple ozone exposure increased the protein expression of NLRP3, the ratio of cleaved-caspase-1 to pro-caspase-1 and the mRNA expression of IL-1β and IL-18 in the lung tissue, evidence for inflammasome activation. The expression levels of NLRP3 and the ratios of cleaved-caspase-1 to pro-caspase-1 were positively correlated with lung inflammation scores, the numbers of caspase-3 positive cells and airway structural changes. The ratios of cleaved-caspase-1

AJRCMB Articles in Press. Published on 05-January-2016 as 10.1165/rcmb.2015-0014OC

to pro-caspase-1 were also positively correlated with emphysematous indices (LAA% and Lm). Furthermore, these effects were prevented and reversed by the preventive and therapeutic treatment with NaHS. This indicates that NaHS treatment inhibited the enhanced activity of NLRP3-caspase-1 axis induced by multiple ozone exposure.

As an important signaling molecule, the p38 mitogen-activated protein kinase (MAPK) is activated in response to many inflammatory signals. The p38 MAPK pathway was upregulated in COPD (37). Other studies have confirmed that there is increased p38 MAPK activation in the lung of COPD patients (38, 39). We showed that the phosphorylation of p38 MAPK was increased and persisted in multiple ozone-induced COPD model. Consistent with other studies that NaHS inhibited the activation of p38 MAPK in lung vascular endothelial cells and airway smooth muscle cells (21, 40), we confirm that preventive or therapeutic treatment with NaHS inhibited and reversed the phosphorylation of p38 MAPK.

Akt (previously referred to as protein kinase B [PKB]) is a molecular mediator of cellular processes central to COPD pathogenesis (41,42). Decreased Akt phosphorylation, which may be related to cell apoptosis and emphysematous development, was observed in the lung of CS-exposed mice (12, 42, 43). NaHS treatment has been shown to activate Akt phoshorylation in lung epithelial cells, lung alveolar epithelial cells and lung vascular endothelial cells (21,44). We showed that the ratios of phospho-Akt/Akt were negatively

correlated with lung inflammation scores, the numbers of caspase-3 positive cells, airway structural changes and emphysema (LAA% and Lm). NaHS prevented and reversed the loss of Akt phosphorylation in our model.

There are several limitations in our study. First, we did not measure the changes in redox regulation in the lung tissue of ozone exposed model. Second, it would have been useful to measure the activity of the inflammasome pathway in airway inflammatory cells or airway structural cells separately so as to ascertain the contribution of each of these cellular compartments. Lastly, in order to prove definitely that NLRP3, p38MAPK and AKt activities are important in underlying the inflammatory process and emphysema induced by ozone exposure, we should have used specific inhibitors or specific knock-out mice to block these pathways. These limitations are currently being considered for future experiments.

In summary, NaHS (an exogenous donor of H_2S) administered prior to each ozone exposure prevented the development of lung inflammation and emphysema, while its administration after multiple ozone exposure reversed lung inflammation and partially reversed features of emphysema in this murine model. The effects of NaHS may be due to the capacity of H_2S in regulating the NLRP3-caspase-1, p38 MAPK and Akt pathways.

AJRCMB Articles in Press. Published on 05-January-2016 as 10.1165/rcmb.2015-0014OC

ACKNOWLEDGEMENTS

This work was supported by grants from the National Nature Science Foundation of China (No.81100024), Shanghai Pujiang Program (No.14PJD027) and Shanghai Health Bureau (No. 20114274) .We would like to thank Mr.Boyin Qin (Shanghai Public Health Clinical Center) for his technical help. Professor Kian Fan Chung is a Visiting Professor of Shanghai Jiao Tong University School of Medicine.

References:

1. Chung KF, Adcock IM. Multifaceted mechanisms in COPD: inflammation, immunity, and tissue repair and destruction. Eur Respir J. 2008;31:1334-1356.

2. Kirkham PA, Barnes PJ. Oxidative stress in COPD. Chest. 2013;144:266-273.

3. Romieu I, Castro-Giner F, Kunzli N, Sunyer J. Air pollution, oxidative stress and dietary supplementation: a review. Eur Respir J. 2008;31:179-197.

4. Medina-Ramon M, Zanobetti A, Schwartz J. The effect of ozone and PM10 on hospital admissions for pneumonia and chronic obstructive pulmonary disease: a national multicity study. Am J Epidemiol 2006;163:579-588.

5. Ko FW, Tam W, Wong TW, Chan DP, Tung AH, Lai CK, Hui DS. Temporal relationship between air pollutants and hospital admissions for chronic obstructive pulmonary disease in Hong Kong. Thorax. 2007;62:780-785.

6. Lee IM, Tsai SS, Chang CC, Ho CK, Yang CY. Air pollution and hospital admissions for chronic obstructive pulmonary disease in a tropical city: Kaohsiung, Taiwan. Inhal toxicol. 2007;19:393-398.

7. Li F, Wiegman C, Seiffert JM, Zhu J, Clarke C, Chang Y, Zhang J, Zhou X, Chung KF. Effects of N-acetylcysteine in ozone-induced chronic obstructive pulmonary disease model. PloS one. 2013;8:e80782.

8. Chung KF. Hydrogen sulfide as a potential biomarker of asthma. Exp Rev Respri Med. 2014;8:5-13.

9. Chen YH, Yao WZ, Geng B, Ding YL, Lu M, Zhao MW, Tang CS.

AJRCMB Articles in Press. Published on 05-January-2016 as 10.1165/rcmb.2015-0014OC

Endogenous hydrogen sulfide in patients with COPD. Chest. 2005;128:3205-3211.

10. Saito J, Mackay AJ, Rossios C, Gibeon D, Macedo P, Sinharay R, Bhavsar PK, Wedzicha JA, Chung KF.Sputum-to-serum hydrogen sulfide ratio in COPD. Thorax. 2014;69:903-909.

11. Chen YH, Wang PP, Wang XM, He YJ, Yao WZ, Qi YF, Tang CS. Involvement of endogenous hydrogen sulfide in cigarette smoke-induced changes in airway responsiveness and inflammation of rat lung. Cytokine. 2011;53:334-341.

12. Han W, Dong Z, Dimitropoulou C, Su Y. Hydrogen sulfide ameliorates tobacco smoke-induced oxidative stress and emphysema in mice. Antioxid & redox signal. 2011;15:2121-134.

13. Tamizhselvi R, Moore PK, Bhatia M. Inhibition of hydrogen sulfide synthesis attenuates chemokine production and protects mice against acute pancreatitis and associated lung injury. Pancreas. 2008;36:e24-e31.

14. Zhang J, Sio SW, Moochhala S, Bhatia M. Role of hydrogen sulfide in severe burn injury-induced inflammation in mice. Mol Med, 2010;16:417-424.

15. Collin M, Anuar FB, Murch O, Bhatia M, Moore PK, Thiemermann C. Inhibition of endogenous hydrogen sulfide formation reduces the organ injury caused by endotoxemia. Bri J Pharmacol. 2005;146:498-505.

16. Esechie A, Kiss L, Olah G, Horvath EM, Hawkins H, Szabo C, Traber DL. Protective effect of hydrogen sulfide in a murine model of acute lung injury

induced by combined burn and smoke inhalation. Clin Sci(Lond). 2008;115:91-97.

17. Chen YH, Wu R, Geng B, Qi YF, Wang PP, Yao WZ, Tang CS. Endogenous hydrogen sulfide reduces airway inflammation and remodeling in a rat model of asthma. Cytokine. 2009;45:117-123.

18. Zhang G, Wang P, Yang G, Cao Q, Wang R. The inhibitory role of hydrogen sulfide in airway hyperresponsiveness and inflammation in a mouse model of asthma. Am J Pathol. 2013;182:1188-1195.

19. Benetti LR, Campos D, Gurgueira SA, Vercesi AE, Guedes CE, Santos KL, Wallace JL, Teixeira SA, Florenzano J, Costa SK, Muscara MN, Ferreira HH. Hydrogen sulfide inhibits oxidative stress in lungs from allergic mice in vivo. European journal of pharmacology. 2013;698:463-469.

20. Zhang P, Li F, Wiegman CH, Zhang M, Hong Y, Gong J, Chang Y, Zhang JJ, Adcock I, Chung KF, Zhou X. Inhibitory Effect of Hydrogen Sulfide on Ozone-induced Airway Inflammation, Oxidative Stress and Bronchial Hyperresponsiveness. Am J Respir Cell Mol Biol.2015;52:129-137.

21. Johnson KA. Imaging techniques for small animal imaging models of pulmonary disease: micro-CT. Toxicol Pathol. 2007;35:59-64.

22. Weibel ER, Hsia CC, Ochs M. How much is there really? Why stereology is essential in lung morphometry. J Appl Physiol. 2007;102:459-467.

23. Froese AR, Ask K, Labiris R, Farncombe T, Warburton D, Inman MD, Gauldie J, Kolb M. Three-dimensional computed tomography imaging in an

AJRCMB Articles in Press. Published on 05-January-2016 as 10.1165/rcmb.2015-0014OC

animal model of emphysema. Eur Respir J. 2007;30:1082-1089.

24. Kawakami M, Matsuo Y, Yoshiura K, Nagase T, Yamashita N. Sequential and quantitative analysis of a murine model of elastase-induced emphysema. Biol Pharm Bull. 2008;31:1434-1438.

25. Stern BR, Raizenne ME, Burnett RT, Jones L, Kearney J, Franklin CA, Air pollution and childhood respiratory health: exposure to sulfate and ozone in 10 Canadian rural communities.Environ. Res. 1994,66: 125-142.

26. Tager IB, Balmes J, Lurmann F, Ngo L, Alcorn S, Kunzli N. Chronic exposure to ambient ozone and lung function in young adults. Epidemiology. 2005;16:751-759.

27. Vanoirbeek JA, Rinaldi M, De Vooght V, Haenen S, Bobic S, Gayan-Ramirez G, Hoet PH, Verbeken E, Decramer M, Nemery B, Janssens W. Noninvasive and invasive pulmonary function in mouse models of obstructive and restrictive respiratory diseases. Am J Respir Cell Mol Biol. 2010;42:96-104.

28. Tyler WS, Tyler NK, Last JA, Gillespie MJ, Barstow TJ. Comparison of daily and seasonal exposures of young monkeys to ozone. Toxicology. 1988; 50:131-144.

29. Harkeman JR, Maunderly JL.Consequences of prolonged inhalation of ozone on F344/N rats: collaborative studies. Part V: effects on pulmonary function. Res Rep Health Eff Inst. 1994;(65 Pt 5):3-17.

30. Kodavanti UP, Hatch GE, Starcher B, Giri SN, Winsett D, Costa

DL.Ozone-induced pulmonary functional, pathological, and biochemical changes in normal and vitamin C-deficientguinea pigs. Fundam Appl Toxicol. 1995;24:154-64.

31. Wang T, Wang L, Zaidi SR, Sammani S, Siegler J, Moreno-Vinasco L, Mathew B, Natarajan V, Garcia JG. Hydrogen sulfide attenuates particulate matter-induced human lung endothelial barrier disruption via combined reactive oxygen species scavenging and Akt activation.Am J Respir Cell Mol Biol. 2012;47:491-496.

32. Birrell MA, Eltom S. The role of the NLRP3 inflammasome in the pathogenesis of airway disease. Pharmacol Therapeut. 2011;130:364-370.

33. Im H, Ammit AJ. The NLRP3 inflammasome: role in airway inflammation. Clin Exp Allergy. 2014;44:160-172.

34. Pauwels NS, Bracke KR, Dupont LL, Van Pottelberge GR, Provoost S, Vanden Berghe T, Vandenabeele P, Lambrecht BN, Joos GF, Brusselle GG. Role of IL-1alpha and the Nlrp3/caspase-1/IL-1beta axis in cigarette smoke-induced pulmonary inflammation and COPD.Eur Respir J. 2011;38:1019-1028.

35. Kang MJ, Homer RJ, Gallo A, Lee CG, Crothers KA, Cho SJ, Rochester C, Cain H, Chupp G, Yoon HJ, Elias JA. IL-18 is induced and IL-18 receptor alpha plays a critical role in the pathogenesis of cigarette smoke-induced pulmonary emphysema and inflammation. J Immunol. 2007;178:1948-1959.

36. Eltom S, Stevenson CS, Rastrick J, Dale N, Raemdonck K, Wong S,

AJRCMB Articles in Press. Published on 05-January-2016 as 10.1165/rcmb.2015-0014OC

Catley MC,Belvisi MG, Birrell MA. P2X7 receptor and caspase 1 activation are central to airway inflammation observed after exposure to tobacco smoke. PloS one. 2011;6(9):e24097.

37. Chung KF. p38 mitogen-activated protein kinase pathways in asthma and COPD. Chest. 2011;139:1470-1479.

38. Renda T, Baraldo S, Pelaia G, Bazzan E, Turato G, Papi A,Maestrelli P, Maselli R, Vatrella A, Fabbri LM, Zuin R, Marsico SA, Saetta M. Increased activation of p38 MAPK in COPD. Eur Respir J. 2008;31:62-69.

39. Gaffey K, Reynolds S, Plumb J, Kaur M, Singh D. Increased phosphorylated p38 mitogen-activated protein kinase in COPD lungs. Eur Respir J. 2013;42(1):28-41.

40. Perry MM, Hui CK, Whiteman M, Wood ME, Adcock I, Kirkham P, Michaeloudes C, Chung KF. Hydrogen sulfide inhibits proliferation and release of IL-8 from human airway smooth muscle cells.Am J Respir Cell Mol Biol, 2011;45:746-752.

41. Bozinovski S, Vlahos R, Hansen M, Liu K, Anderson GP. Akt in the pathogenesis of COPD. Int J Chronic Obstr. 2006;1:31-38.

42. Marwick JA, Edirisinghe I, Arunachalam G, Stevenson CS, Macnee W, Kirkham PA, Rahman I. Cigarette smoke regulates VEGFR2-mediated survival signaling in rat lungs. J Inflamm (Lond). 2010; 7: 11.

43. Kim SY, Lee JH, Huh JW, Ro JY, Oh YM, Lee SD, An S, Lee YS. Cigarette smoke induces Akt protein degradation by the ubiquitin-proteasome system.J

Bio Chem. 2011;286:31932-31943.

44. Madurga A, Mizikova I, Ruiz-Camp J, Vadasz I, Herold S, Mayer K, Fehrenbach H, Seeger W, Morty RE. Systemic hydrogen sulfide administration partially restores normal alveolarization in an experimental animal model of bronchopulmonary dysplasia. Am J Physiol Lung Cell Mol Physiol. 2014;306:L684-697.

AJRCMB Articles in Press. Published on 05-January-2016 as 10.1165/rcmb.2015-0014OC

FIGURE LEGENDS

Figure 1. Representative picture of the three-dimensional images of lungs of PBS-pretreated air-exposed mice (Panel A), NaHS-pretreated air-exposed mice (Panel B),PBS-pretreated ozone-exposed mice (Panel C), NaHS-pretreated ozone-exposed mice (Panel d), air-exposed PBS-treated mice (Panel E), air-exposed NaHS-treated mice (Panel F), ozone-exposed PBS-treated mice (Panel G), ozone-exposed NaHS-treated mice (Panel H). Red color represents low attenuation area (LAA), i.e, voxels with densities -700– -550HU. Although the trachea and bronchi are shown as red areas in this figure, these were removed from calculation of LAA. Panel I. Individual and mean values of total lung volume in the preventive groups. Panel J. Individual and mean values of total lung volume in the therapeutic groups. Panel K. Individual and mean LAA% in the preventive groups. Panel L Individual and mean LAA% in the therapeutic groups. *P<0.05, **P<0.01, *** P<0.001.

Figure 2. Representative photomicrographs of lung alveolar spaces and mean linear intercept (L_m) in haematoxylin-eosin-stained sections of PBS-pretreated air-exposed mice (Panel A),NaHS-pretreated air-exposed mice (Panel B), PBS-pretreated ozone-exposed mice (Panel C), NaHS-pretreated ozone exposed mice(Panel D), air-exposed PBS-treated mice (Panel E), air-exposed NaHS-treated mice(Panel F),ozone-exposed PBS-treated mice (Panel G) ozone-exposed NaHS-treated mice (Panel H). (bar=25 μm). Panel I,Individual and mean values of Lm in the lung sections from the preventive groups. Panel J.Individual and mean values of Lm in the lung sections from the therapeutic

groups.*P<0.05, **P<0.01, *** P<0.001.

Figure 3. Individual and mean values of inspiratory capacity (IC)(Panel A),functional residual capacity (FRC) (Panel B),total lung capacity (TLC) (Panel C), chord compliance (Cchord) (Panel D), and percentage of forced expiratory volume (FEV) in first 25 and 50 ms of fast expiration (FEV_{25} and FEV_{50}) of forced vital capacity (FVC)(Panels E,F). *P<0.05, **P<0.01, ***P<0.001. P, preventive groups, T, therapeutic groups.

Figure 4. Individual and mean numbers of total cells (TOTAL) (Panel A), macrophages (MAC) (Panel B), lymphocytes (LYM) (Panel C), neutrophils (NEU) (Panel D) and eosinophils (EOS) (Panel E) in bronchoalveolar lavage (BAL) fluid for the 6 experimental groups. Panel F. Individual and mean inflammation scores in the airways and lungs. Panel G. Individual and mean concentrations of malonaldehyde in bronchoalveolar lavage fluid. Panel H. Mean values of serum 8-hydroxy-deoxyguanosine (8-OHdG) *P<0.05, **P<0.01. P, preventive groups, T, therapeutic groups.

Figure 5. Individual and mean values of thickness of airway epithelial layer (Wae/Pbm) (Panel A), airway smooth muscle (Wam/Pbm) (Panel B) and total airway wall (Panel C) in the bronchial wall. Panel D. Individual and mean values of caspase-3 positive cells in the lung parenchyma from the 8

AJRCMB Articles in Press. Published on 05-January-2016 as 10.1165/rcmb.2015-0014OC

experimental groups. $^{*}P<0.05$, $^{**}P<0.01$, *** $P<0.001$. P, preventive groups, T, therapeutic groups.

Figure 6. Individual and mean fold-change in mRNA expression of IL-1β (Panel A), IL-18 (Panel B), MMP-9 (Panel C), SOD2 (Panel D) and HO-1(Panel E) in lung tissue measured by quantitative RT-PCR. $^{*}P<0.05$, $^{**}P<0.01$, *** $P<0.001$. P, preventive groups, T, therapeutic groups.

Figure 7. Western blot analysis of the relative protein expression of NLRP3 to GAPDH (Panel A), the ratio of cleaved capsase-1 to pro-caspase-1(Panel B), the ratio of phosphorylated p38 mitogen-activated protein kinase (MAPK) to nonphosphoryated p38 MAPK (Panel C) and phosphorylated Akt to nonphosphoryated Akt (Panel D) in the lung tissue. Each panel shows representative Western blot. $^{*}P<0.05$, $^{**}P<0.01$, *** $P<0.001$. P, preventive groups, T, therapeutic groups.

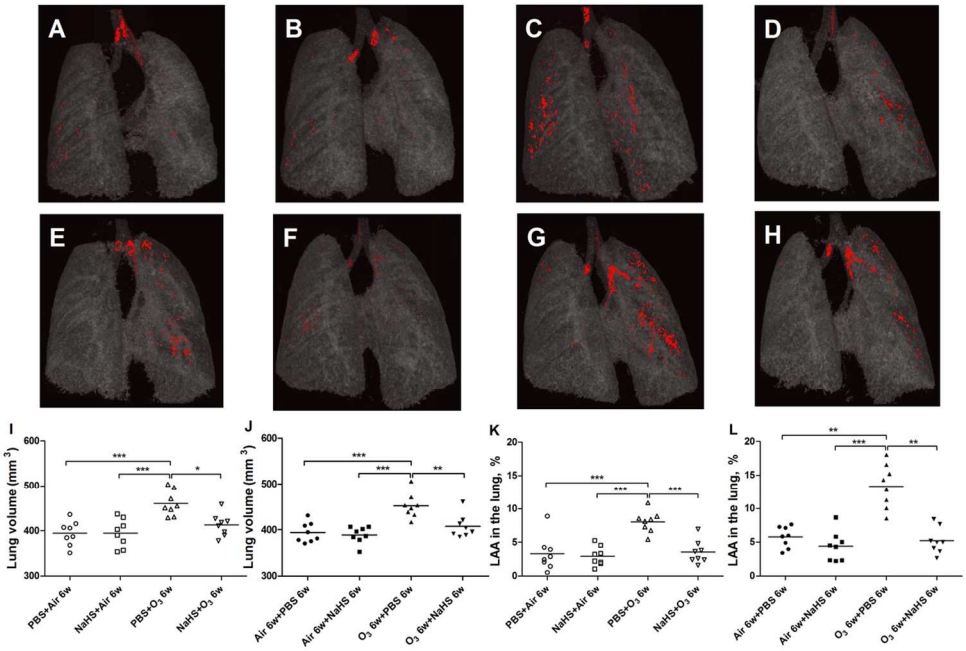

Figure 1. Representative picture of the three-dimensional images of lungs of PBS-pretreated air-exposed mice (Panel A), NaHS-pretreated air-exposed mice (Panel B),PBS-pretreated ozone-exposed mice (Panel C), NaHS-pretreated ozone-exposed mice (Panel d), air-exposed PBS-treated mice (Panel E), air-exposed NaHS-treated mice (Panel F), ozone-exposed PBS-treated mice (Panel G), ozone-exposed NaHS-treated mice (Panel H). Red color represents low attenuation area (LAA), i.e, voxels with densities -700– -550HU. Although the trachea and bronchi are shown as red areas in this figure, these were removed from calculation of LAA. Panel I. Individual and mean values of total lung volume in the preventive groups. Panel J. Individual and mean values of total lung volume in the therapeutic groups. Panel K. Individual and mean LAA% in the preventive groups. Panel L Individual and mean LAA% in the therapeutic groups. *P<0.05, **P<0.01, *** P<0.001.
118x81mm (300 x 300 DPI)

AJRCMB Articles in Press. Published on 05-January-2016 as 10.1165/rcmb.2015-0014OC

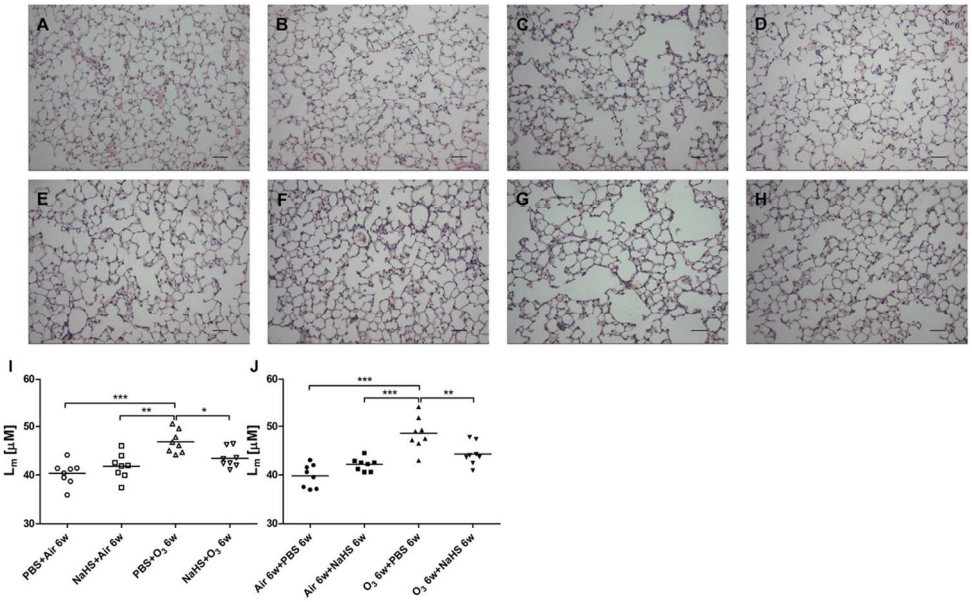

Figure 2. Representative photomicrographs of lung alveolar spaces and mean linear intercept (Lm) in haematoxylin-eosin-stained sections of PBS-pretreated air-exposed mice (Panel A),NaHS-pretreated air-exposed mice (Panel B), PBS-pretreated ozone-exposed mice (Panel C), NaHS-pretreated ozone exposed mice(Panel D), air-exposed PBS-treated mice (Panel E), air-exposed NaHS-treated mice(Panel F),ozone-exposed PBS-treated mice (Panel G) ozone-exposed NaHS-treated mice (Panel H). (bar=25 µm). Panel I,Individual and mean values of Lm in the lung sections from the preventive groups. Panel J.Individual and mean values of Lm in the lung sections from the therapeutic groups.*P<0.05, **P<0.01, *** P<0.001.
109x70mm (300 x 300 DPI)

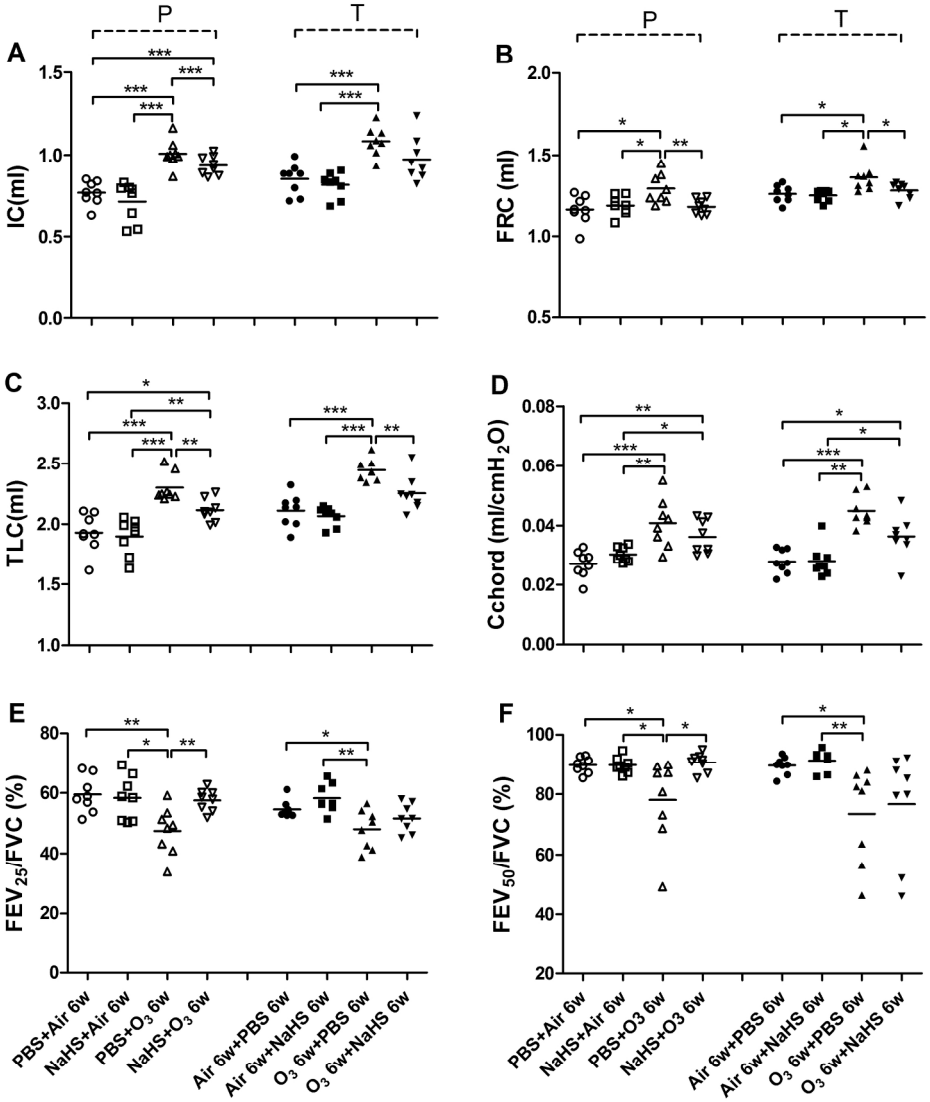

Figure 3. Individual and mean values of inspiratory capacity (IC)(Panel A),functional residual capacity (FRC) (Panel B),total lung capacity (TLC) (Panel C), chord compliance (Cchord) (Panel D), and percentage of forced expiratory volume (FEV) in first 25 and 50 ms of fast expiration (FEV25 and FEV50) of forced vital capacity (FVC)(Panels E,F). *P<0.05, **P<0.01, ***P<0.001. P, preventive groups, T, therapeutic groups.
206x249mm (300 x 300 DPI)

AJRCMB Articles in Press. Published on 05-January-2016 as 10.1165/rcmb.2015-0014OC

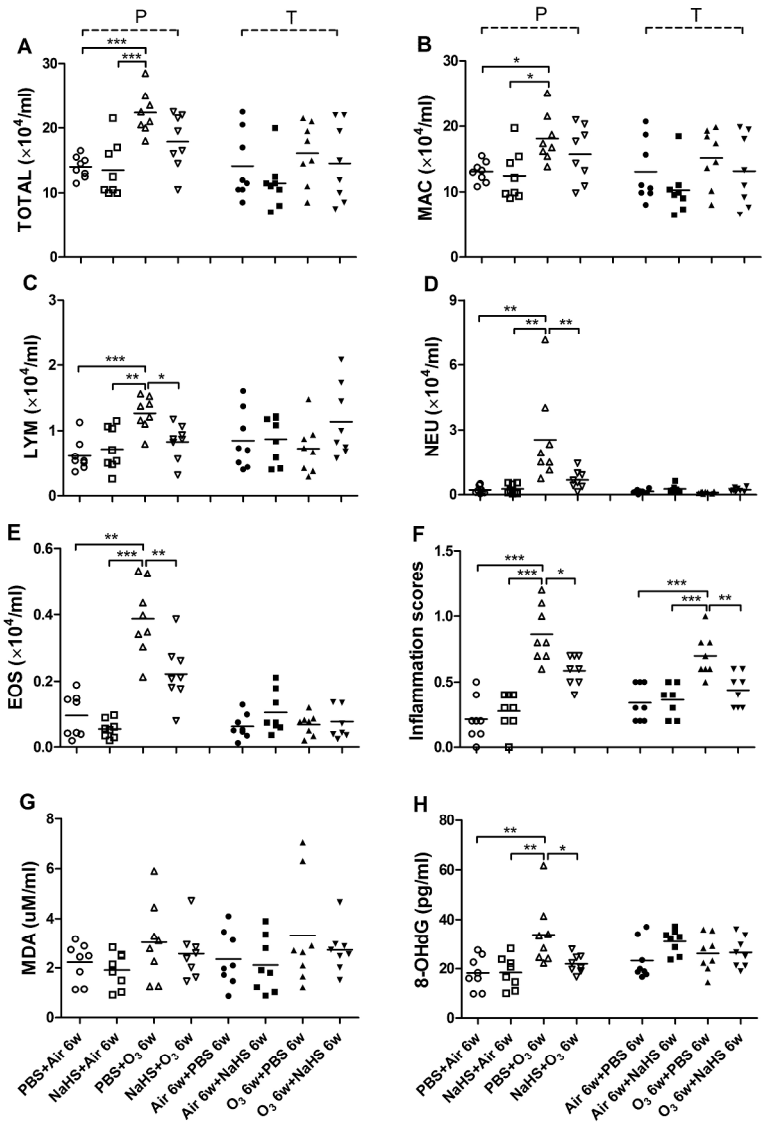

Figure 4. Individual and mean numbers of total cells (TOTAL) (Panel A), macrophages (MAC) (Panel B), lymphocytes (LYM) (Panel C), neutrophils (NEU) (Panel D) and eosinophils (EOS) (Panel E) in bronchoalveolar lavage (BAL) fluid for the 6 experimental groups. Panel F. Individual and mean inflammation scores in the airways and lungs. Panel G. Individual and mean concentrations of malonaldehyde in bronchoalveolar lavage fluid. Panel H. Mean values of serum 8-hydroxy-deoxyguanosine (8-OHdG) *P<0.05, **P<0.01. P, preventive groups, T, therapeutic groups.
250x368mm (300 x 300 DPI)

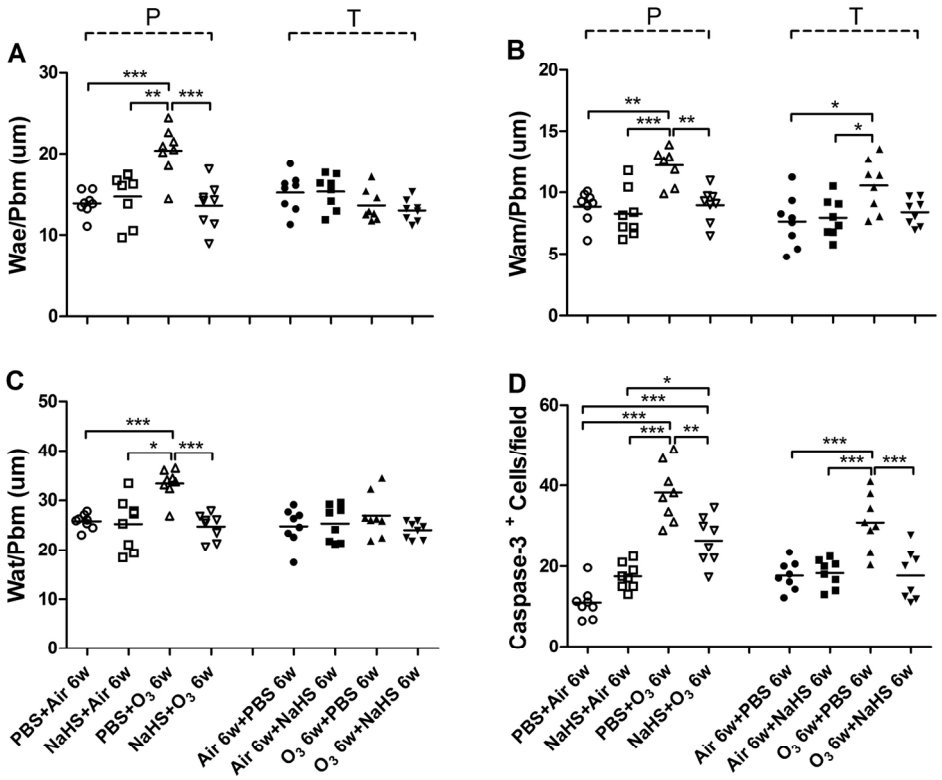

Figure 5. Individual and mean values of thickness of airway epithelial layer (Wae/Pbm) (Panel A), airway smooth muscle (Wam/Pbm) (Panel B) and total airway wall (Panel C) in the bronchial wall. Panel D. Individual and mean values of caspase-3 positive cells in the lung parenchyma from the 8 experimental groups. *P<0.05, **P<0.01, *** P<0.001. P, preventive groups, T, therapeutic groups.
149x131mm (300 x 300 DPI)

AJRCMB Articles in Press. Published on 05-January-2016 as 10.1165/rcmb.2015-0014OC

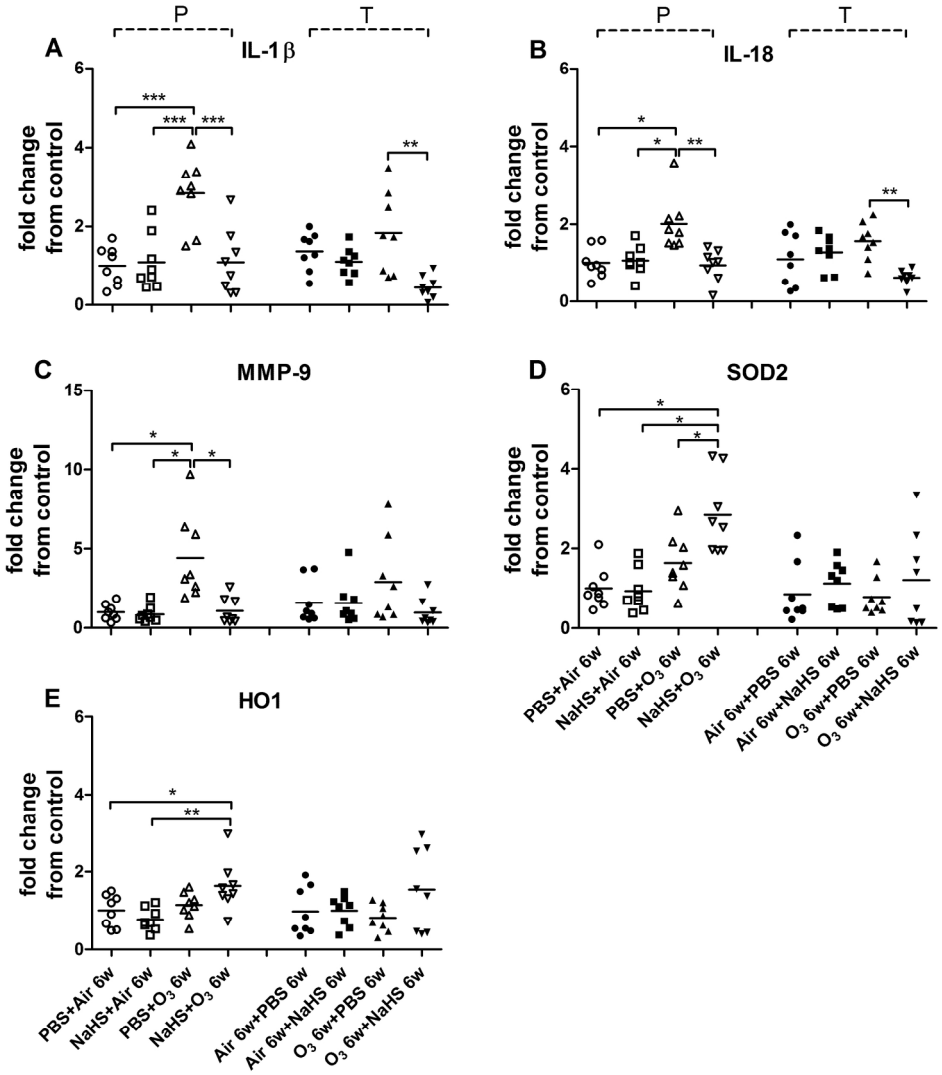

Figure 6. Individual and mean fold-change in mRNA expression of IL-1β (Panel A), IL-18 (Panel B), MMP-9 (Panel C), SOD2 (Panel D) and HO-1(Panel E) in lung tissue measured by quantitative RT-PCR. *P<0.05, **P<0.01, *** P<0.001. P, preventive groups, T, therapeutic groups.
198x231mm (300 x 300 DPI)

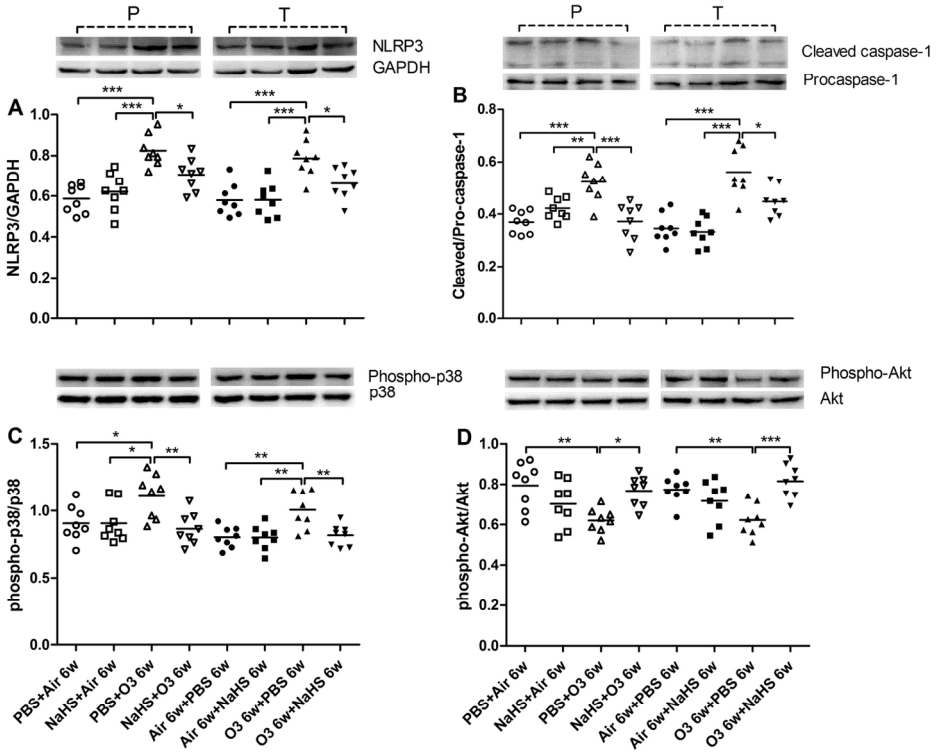

Figure 7. Western blot analysis of the relative protein expression of NLRP3 to GAPDH (Panel A), the ratio of cleaved capsase-1 to pro-caspase-1(Panel B), the ratio of phosphorylated p38 mitogen-activated protein kinase (MAPK) to nonphosphoryated p38 MAPK (Panel C) and phosphorylated Akt to nonphosphoryated Akt (Panel D) in the lung tissue. Each panel shows representative Western blot. *P<0.05, **P<0.01, *** P<0.001. P, preventive groups, T, therapeutic groups.
142x119mm (300 x 300 DPI)

AJRCMB Articles in Press. Published on 05-January-2016 as 10.1165/rcmb.2015-0014OC

Online Supplement

Hydrogen sulfide prevents and partially reverses ozone-induced features of chronic obstructive pulmonary disease

Feng Li[1*], Pengyu Zhang[1*], Min Zhang[1*], Li Liang[3], Xiaoyuan Sun[1], Min Li[2],Yueqin Tang[2], Aihua Bao[1], Jicheng Gong[4], Junfeng (Jim) Zhang[4], Ian Adcock[5], Kian Fan Chung[5], Xin Zhou[1#]

*These authors contributed equally to this work.

[#]Corresponding author:

Professor Xin Zhou

Dept of Respiratory Medicine,

Shanghai First People's Hospital, Shanghai Jiao Tong University.

No.100, Haining Road, Shanghai, 200080, China.

E-mail: xzhou53@163.com

Telephone number: 0086 21 63071428

Fax number: 0086 21 63071428

Material and Methods

Ozone exposure

Pathogen-free, 8-10 week old male C57/BL6 mice (Shanghai Super -- B&K laboratory animal Corp.Ltd, Shanghai,China) were housed in specific-pathogen-free (SPF) conditions under a constant temperature (20 °C) and relative humidity (40%~60%) with food and water supplied ad libitum. All experimental procedures involving animals were approved by the Laboratory Animal Ethics Committee of the institute.

Mice were exposed to ozone produced from a generator (Model 300, AB Aqua Medic GmbH, Bissendorf, Germany), mixed with air for 3 hours at a concentration 2.5 parts per million (ppm) in a sealed Perspex container[S1]. Ozone concentration was continuously monitored and maintained using an ozone switch (OS-4, EcoSensors Division, KWJ Engeneering, Inc., Newark, NJ, USA). Control animals were exposed to filtered air only. The experiment was carried out in 8 groups (Supplementary Fig 1). For groups 1-4, the mice were injected intraperitoneally with either NaHS (2 mg/kg; dissolved in phosphate-buffered saline, PBS) or vehicle alone (PBS) one hour before each exposure to either ozone or air, two exposures (every 3 days) per week for 6 weeks. For groups 5-8, following the cessation of ozone/air exposure, the mice were injected intraperitoneally with either NaHS (2 mg/kg; dissolved in PBS) or vehicle alone (PBS), two times (every 3 days) per week for 6 weeks.

Micro-computed tomography (micro-CT)

Mice were anesthetised with pentobarbital sodium (1mg/Kg) and placed in the chamber of the Micro-CT eXplore Locus (GE healthcare, London, Ontario, Canada)[S2]. X-ray tube was set at 50 kV with current of 450uA. A total of 515 projections were acquired with a 0.5° angular increment during a 360° circular orbit, with effective pixel size of 0.092 mm. Exposure time was 300ms per projection, slice thickness was 93μm and field of view was 80×45mm. Images were reconstructed using reconstruction utility, and were then analyzed using

AJRCMB Articles in Press. Published on 05-January-2016 as 10.1165/rcmb.2015-0014OC

Microview 2.0 +ABA software (GE Healthcare, London, Ontario, Canada) to quantify lung tissue density. Three-dimensional volumes were drawn manually around the anatomical lungs in each image. The low attenuation area (LAA) was set in the range of -750 to -550 Hounsfield Units (HU). The percentage of LAA was calculated using the ratio of the total LAA volume to the total lung volume.

Forced maneuver system

Mice were tracheostomized and placed in a whole-body plethysmograph and connected to a computer-controlled ventilator (Buxco,Wilmington, NC,USA), with an average breathing frequency of 150 breaths/min[S1]. Functional residual capacity (FRC) was determined by Boyle's law, and the chord compliance (Cchord), a measure of the compliance on expiration between 0-10 cmH2O of pressure, was determined from the quasi-static pressure-volume maneuver. From quasi-static pressure-volume loops, inspiratory capacity (IC), total lung capacity (TLC), forced vital capacity (FVC) and the forced expiratory volume in first 20 and 50 milliseconds of exhalation (FEV_{25}, FEV_{50}) were recorded during fast flow volume maneuver. Three acceptable maneuvers were conducted for all numeric parameters for each test in every mouse.

BAL fluid, blood collection and cell counting

Following terminal anaesthesia with pentobarbitone, mice were lavaged with two 0.8 ml aliquots of PBS via an endotracheal tube. Blood was taken from the heart through a syringe and collected into tubes, then left to clot at 4ºC followed by centrifugation at 5000 rpm for 10 min. The serum was collected and stored at -80 ºC. The BAL fluid was centrifuged at 4ºC, 1500 rpm for 10 min, the supernatant was stored and cell pellet was re-suspended in PBS. Total cell counts were determined using a hemocytometer, and differential cell counts from cytospin preparations stained by Liu's stain solution

(Baso Diagnostics Inc, Zhuhai, China) were determined under an Olympus microscope (Olympus Optical Company Ltd., Tokyo, Japan). At least 500 cells were counted and identified as macrophages, eosinophils, lymphocytes or neutrophils according to standard morphology.

MDA measurement

MDA was measured using a HPLC system with fluorescent detection (Waters, Milford, MA, USA). A 20 µl aliquot sample was added into a mixture of 500 µl phosphoric acid (440 mM) and 250 µl thiobarbituricacid (TBA, 42 mM). After 1-hour reaction with TBA at 80°C in an oven, a 20 µl aliquot of this final solution was injected into the HPLC system with fluorescence detector set at 532 nm for the excitation wavelength and 553 nm for the emission wavelength. A Nova-Pak C18 column (Waters, Milford, MA, USA) was used with a mobile phase that was composed of 40% methanol and 60% water containing 50mM KH2PO4 (pH=6.8) at a flow rate of 0.8 ml/min. The detection limit, extraction recovery and analytical precision of this method were 1.8 nM, 75.9%, and 2.2% (measured as RSD from 8 replicate injections), respectively.

Serum 8-hydroxy-2'-deoxyguanosine (8-OHdG)

For 8-OHdG analysis, a serum sample was diluted with 1 mL of 0.1M KH_2PO_4 (pH=6.0), vortexed and centrifuged, purified using a Sep-Pak C18 cartridge (Waters, Milford, MA, USA), and then analyzed on a TSQ Quantum Access MAX triple stage quadrupole mass spectrometer (Thermo Fisher Scientific, San Jose, CA, USA). Chromatographic separation was achieved using a 150 mmx2.1mm Alltima HP HILIC column (Grace Davison Discovery Sciences, Deerfield, IL, USA) and a gradient elution program. The mass spectrometer was operated in the positive ESI mode. The ion pairs of m/z 284/168 and m/z 289/173 were used to quantify 8-OHdG and $^{15}N_5$-8-OHdG, respectively. The method detection limit, recovery and analytical variability was 10 pg/ml, 96.5% and 8.2%, respectively.

AJRCMB Articles in Press. Published on 05-January-2016 as 10.1165/rcmb.2015-0014OC

Histological analysis

The whole lung was removed from the chest and the right lung lobes were dissected and snap frozen in liquid nitrogen for later analysis. The left lung was inflated with 4% paraformaldehyde under 25-cm of water pressure and then embedded in paraffin. Paraffin blocks were sectioned to expose the maximum surface area of lung tissue in the plane of the bronchial tree. Five μm sections were cut and stained with haematoxylin and eosin (H&E). All counts were performed by observers who were blinded as to the mice studied.

The mean linear intercept (Lm), a measure of interalveolar septal wall distance, was determined using a reticule with 5 lines (each 500 μM long), with 10 fields per section assessed at random. Two H&E stained slides per mouse were coded and analyzed. Fields with airways or vessels were avoided by moving one field in any one direction. The mean linear intercept was calculated through dividing the length of the line by the number of alveolar wall and grid line interception counted.

Lung inflammation was scored on a 0–3 scale[S3]: 0, no inflammation was detectable; 1, occasional cuffing with inflammatory cells; 2, most bronchi or vessels were surrounded by a thin layer (one to five cells thick) of inflammatory cells; 3, most bronchi or vessels were surrounded by a thick layer (more than five cells thick) of inflammatory cells. Total lung inflammation was defined as the average of the peribronchial and perivascular inflammation scores.

Bronchial structure analysis

To assess the structural changes in the airway, the area of airway epithelium (Wae), airway smooth muscle (Wam) and total airway wall (Wat), and the perimeter of basement membrane (Pbm) was measured in H&E stained section. The thickness of above morphological changes was calculated as Wae/Pbm, Wam/Pbm and Wat/Pbm. Morphometric analysis was conducted using Motic digital microscope image analysis system (Motic China

Group, Xiamen, Fujian, China). A minimum of five fields per slice was randomly examined for analysis.

Immunostaining for active caspase-3

After treatment with 3% hydrogen peroxide in methanol for 10 minutes and normal goat serum for 30 minutes, sections were incubated with the polyclonal rabbit anti-active caspase-3 (Cell Signaling Technology, Beverly, CA, USA) overnight. The next day, sections were incubated with goat anti-rabbit horseradish peroxidase (HRP)-conjugated secondary antibody (ICLLAB,Portland,OR,USA) followed by incubation with diaminobenzidine (DAB) and counterstained with Mayer's hematoxylin to provide nuclear and morphological detail. Irrelevant rabbit IgG was used for the primary layer as a negative control procedure. The number of active caspase-3 positively stained alveolar septal cell per field was also counted under microscope (400×magnification). All counts on histology sections were performed by two investigators who were unaware of the treatment protocol of the mouse sections.

PCR

Total RNA was extracted from frozen stored lung tissue using Trizol. The cDNA generated through MMLV reverse transcriptase (Promega, Madison, Wisconsin, USA) was used as template in real-time PCR analyses by using SYBR Green PCR Supermix Reagent (ShineGene, Shanghai, China) and Step one plus system(Life Technologies, South San Francisco, CA,USA).Sequences of primers were designed using Primer 3 software online from Simgene and assessed using the BLAST software. Melting curve analysis was carried out to ensure the presence of one specific PCR product. The sequences of the gene specific primer sets were:

IL-1β F: GTA CAA GGA GAA CCA AGC A, R: CCG TCT TTC ATT ACA CAG G,

IL-18 F: AGG ACA CTT TCT TGC TTG C,R: CAC AAA CCC TCC CCA CCT A,

AJRCMB Articles in Press. Published on 05-January-2016 as 10.1165/rcmb.2015-0014OC

MMP-9 F: CTA AAC CAC CTC TCC CGA C, R: CCC GAC ACA CAG TAA GCA T,
SOD2 F: TTA CAA CTC AGG TCG CTC T, R: CAA CTC TCC TTT GGG TTC T,
HO-1 F: ATG TTG ACT GAC CAC GAC T, R: GAT AGC CCC ACT TTG TTA G,
Beta-actin F: CCT CTA TGC CAA CAC AGT , R: AGC CAC CAA TCC ACA CAG 3,

PCR conditions were as follows: initial heat activation, 10 min at 95°C; denaturation, 15 s at 95°C; annealing, 30 s at 60°C; extension, 20 s at 80°C; 40 cycles. Results from the reaction were analyzed and relative abundance of gene expression was normalized to beta-actin expression.

Western blot

Frozen lung tissues were homogenized in RIPA buffer (Beyotime, Jiangsu, China) and quantified by BCA analysis (Thermos Scientific). Equal amounts of protein were separated by SDS-PAGE and electrophoretically transferred to nitrocellulose membranes. The membranes were incubated in blocking solution at room temperature for 1h and then incubated with primary antibodies against phospho-p38 MAPK, phospho-Akt (Cell Signaling Technology, Beverly, CA, USA), NLRP3 and caspase-1 overnight at 4 ºC. A horseradish peroxidase-conjugated anti-rabbit secondary antibody (diluted to 1:2000 from Cell Signaling Technology) was used, and enhanced chemiluminescence reagent (GE Healthcare, Little Chalfont, Buckinghamshire, UK) was used for detection. The density was quantitated using Bio-Rad Quantity One Software. The blots were stripped and then re-probed with antibodies to GAPDH (Cell Signaling Technology), total p38 MAPK and total Akt (Cell Signaling Technology, Beverly, CA, USA). Band densities were quantified using a densitometer.

Results and Figures

1.Supplementary Figure 1. Protocol used in the eight experimental groups.

2.Supplementary Figure 2. Representative immunohistochemical staining of the active caspase-3 positive cells in parenchyma of PBS-pretreated air-exposed mice (Panel A), NaHS-pretreated air-exposed mice (Panel B),PBS-pretreated ozone-exposed mice (Panel C), NaHS-pretreated ozone-exposed mice (Panel D), air-exposed PBS-treated mice (Panel E), air-exposed NaHS-treated mice (Panel F), ozone-exposed PBS-treated mice (Panel G), ozone-exposed NaHS-treated mice (Panel H). (bar=50 μm)

Reference:

S1. Li F, Wiegman C, Seiffert JM, Zhu J, Clarke C, Chang Y, et al. Effects of N-acetylcysteine in ozone-induced chronic obstructive pulmonary disease model. PloS one. 2013;8(11):e80782.

S2. Froese AR, Ask K, Labiris R, Farncombe T, Warburton D, Inman MD, et al. Three-dimensional computed tomography imaging in an animal model of emphysema. Eur Respir J. 2007;30(6):1082-1089.

S3. Braber S, Henricks PA, Nijkamp FP, Kraneveld AD, Folkerts G. Inflammatory changes in the airways of mice caused by cigarette smoke exposure are only partially reversed after smoking cessation. Respir Res 2010;11: 99.

AJRCMB Articles in Press. Published on 05-January-2016 as 10.1165/rcmb.2015-0014OC

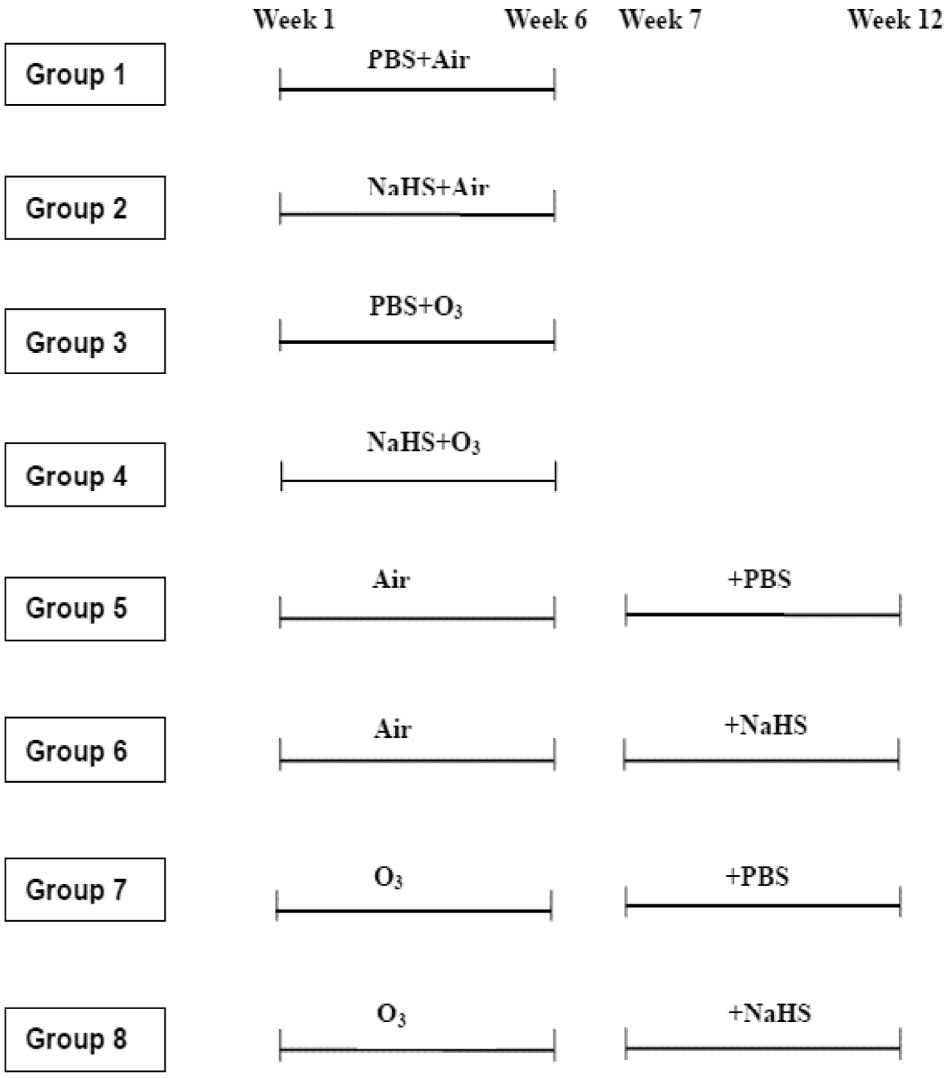

1.Supplementary Figure 1. Protocol used in the eight experimental groups.
139x162mm (600 x 600 DPI)

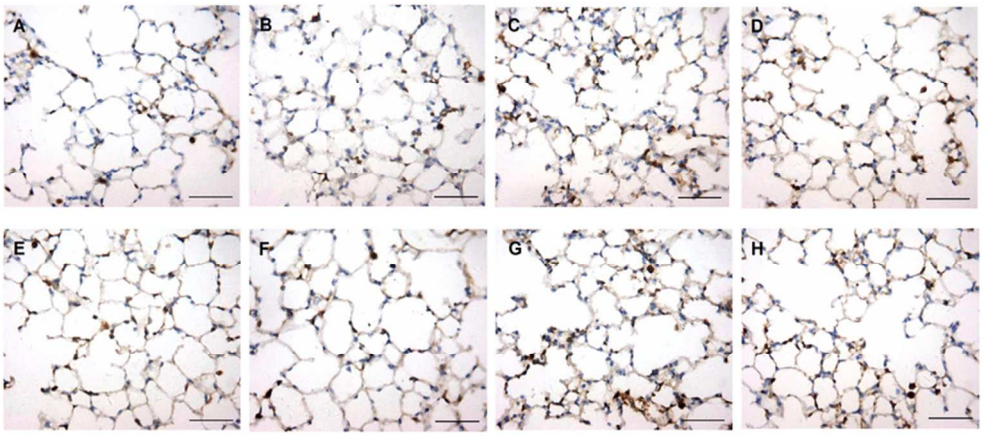

2.Supplementary Figure 2. Representative immunohistochemical staining of the active caspase-3 positive cells in parenchyma of PBS-pretreated air-exposed mice (Panel A), NaHS-pretreated air-exposed mice (Panel B),PBS-pretreated ozone-exposed mice (Panel C), NaHS-pretreated ozone-exposed mice (Panel D), air-exposed PBS-treated mice (Panel E), air-exposed NaHS-treated mice (Panel F), ozone-exposed PBS-treated mice (Panel G), ozone-exposed NaHS-treated mice (Panel H). (bar=50 μm)
77x34mm (300 x 300 DPI)